Journal of Catalysis 292 (2012) 148–156

Contents lists available at SciVerse ScienceDirect

Journal of Catalysis

journal homepage: www.elsevier.com/locate/jcat

Gold nanoparticles supported on magnesium oxide as catalysts for the aerobic oxidation of alcohols under alkali-free conditions

Vinícius V. Costa [a], Miguel Estrada [b], Yulia Demidova [c], Igor Prosvirin [c], Vladimir Kriventsov [c], Rafaela F. Cotta [a], Sergio Fuentes [d], Andrey Simakov [d], Elena V. Gusevskaya [a,*]

[a] Departamento de Química, Universidade Federal de Minas Gerais, 31270-901 Belo Horizonte, MG, Brazil
[b] Posgrado en Física de Materiales, Centro de Investigación Científico y de Educación Superior de Ensenada, C.P. 22860 Ensenada, B.C., Mexico
[c] Boreskov Institute of Catalysis, Lavrentieva 5, Novosibirsk 630090, Russia
[d] Universidad Nacional Autónoma de México, Centro de Nanociencias y Nanotecnología, Km. 107 Car. Tijuana a Ensenada, C.P. 22860 Ensenada, B.C., Mexico

ARTICLE INFO

Article history:
Received 27 March 2012
Revised 8 May 2012
Accepted 9 May 2012
Available online 14 June 2012

Keywords:
Gold catalysts
Selective oxidation
Oxygen
Benzyl alcohol
Monoterpenic alcohols

ABSTRACT

Gold nanoparticles supported on magnesium oxide were shown to be efficient heterogeneous catalysts for the liquid-phase oxidation of a wide range of alcohols using molecular oxygen as a sole oxidant in the absence of co-catalysts or additives. The Au/MgO material was prepared through the deposition–precipitation method and characterized by XRD, XPS, XAS, HRTEM, UV–Vis spectroscopy, and N_2 adsorption techniques. The formation of gold nanoparticles on the MgO surface under temperature programmed reduction was monitored by *in situ* UV–Vis–Mass spectroscopy. Various carbonylic monoterpenoids important for fragrance and pharmaceutical industries were obtained in good to excellent yields starting from biomass-based monoterpenic alcohols, such as isoborneol, perillyl alcohol, and carveol. The Au/MgO catalyst also performs a selective one-pot oxidative esterification of benzyl alcohol in alkali-free methanol solutions in the absence of any additive to give methyl benzoate in a virtually quantitative yield.

1. Introduction

The oxidation of alcohols is one of the most challenging reactions in synthetic organic chemistry. The resulting carbonyl compounds are widely employed in various fields of chemical industry; however, many commonly used processes are still based on stoichiometric oxidation reactions which produce large amounts of wastes [1]. For these reasons, metal catalyzed oxidations of alcohols, especially those that involve molecular oxygen as a final oxidant, currently attract much attention. Various homogeneous [2,3] and heterogeneous [4–9] transition metal catalysts have been reported for the aerobic oxidation of alcohols, with gold nanoparticles (NPs) being among the most promising ones [10–23].

The oxidation of alcohols over gold catalysts often requires the presence of base to promote the abstraction of hydrogen from the substrate and to capture free carboxylic acid formed at the reaction, which could poison the catalyst [12]. Nevertheless, several gold-containing catalysts have been developed for the aerobic oxidation of alcohols under base-free conditions [14–23]. One of the recently suggested approaches to prevent the consumption of base in stoichiometric amounts due to the formation carboxylic acid salts is performing the reaction in methanol solutions [24–30]. In these systems, carboxylic acids are trapped by methanol, which itself is rather inert to aerobic oxidation, so that methyl esters are formed as final products.

Methyl esters find a commercial use as solvents, diluents, extractants, and flavoring agents. Their syntheses commonly consist in two-step procedures that include the esterification of carboxylic acids or their derivatives obtained in a separate step. Only a few catalysts capable to promote direct transformations of alcohols into methyl esters using molecular oxygen as a final oxidant have been reported, with all of them being based on gold NPs, as far as we know [24–30]. In a previous work, we found that gold NPs supported on Ce- or Ti-modified hexagonal mesoporous silica (HMS) efficiently performed the one-pot aerobic oxidative esterification of benzyl alcohol [30]. However, the systems were active only in the presence of the base co-catalyst (potassium carbonate), likewise most of other gold systems reported for the oxidative esterification of alcohols. One of a few examples of the synthesis of carboxylic esters from alcohols under neutral conditions involves the use of gold NPs supported on nanocrystalline β-Ga_2O_3 [28]. It has been suggested that the Au/β-Ga_2O_3 acts as a bifunctional catalyst due to the increased surface Lewis acidity of the support.

* Corresponding author. Fax: +55 31 34095700.
E-mail address: elena@ufmg.br (E.V. Gusevskaya).

0021-9517/$ - see front matter © 2012 Elsevier Inc. All rights reserved.
http://dx.doi.org/10.1016/j.jcat.2012.05.009

In the present work, we have prepared the material containing gold NPs supported on the magnesium oxide and studied its activity in the aerobic oxidation of various alcohols. The formation of NPs on the MgO surface has been monitored by *in situ* UV–Vis–Mass spectroscopy as it is well established that catalytic properties of gold NPs are strongly related to the appropriate preparation procedure [13].

The obtained Au/MgO sample showed high catalytic activity in the aerobic oxidative esterification of benzyl alcohol in the absence of base or any other additive. The oxidation of alcohols under base-free conditions catalyzed by gold NPs supported on magnesium oxide has been described by several groups [14,17–21]. However, to the best of our knowledge, no data on the applications of these materials for the oxidative methoxylation of alcohols have been previously reported.

The catalyst was also tested in the aerobic oxidation of natural monoterpenic alcohols. Terpenic compounds, in general, are biomass-based renewable substrates widely used in the flavor and fragrance industry, which is essentially based on the chemistry of terpenes. For several years, we have been interested in catalytic oxidations of natural products, including terpenes, over ruthenium [9], cobalt [31,32], palladium [33–35], and chromium [36] catalysts. In continuation of our ongoing project aimed at adding value to natural ingredients of essential oils, we report herein the additive-free aerobic oxidation of various monoterpenic alcohols catalyzed by Au/MgO to give valuable fragrance aldehydes and ketones.

2. Experimental

2.1. Catalyst preparation

Gold (3 wt.%) was supported by deposition–precipitation using urea as a precipitation agent as in [37]. MgO (4.0 g, Mallinckrodt) was added to an aqueous solution (400 mL) of $HAuCl_4$ (1.6×10^{-3} M) and urea (0.42 M). The initial pH of the solution was ca. 2. The suspension was vigorously stirred at 80 °C for 4 h. Then, the solid material was filtered and washed with ammonium hydroxide (25.0 M) for 30 min. The last procedure developed in [38] is quite effective to stabilize small gold NPs. After stirring with ammonium hydroxide, the pH of the solution was ca. 10. Finally, the sample was washed with water until the pH of the solution reached the value of 7, then filtered, and dried at room temperature for 24 h. This sample, denoted as the freshly prepared Au/MgO catalyst, was then reduced in the flow of H_2 (5 vol.%), Ar (5 vol.%), and He (balance) (50 mL min^{-1}) at a heating rate of 20 °C min^{-1} up to 350 °C, and the resulting material, denoted as the reduced Au/MgO catalyst, was used in catalytic tests.

2.2. Catalyst characterization

Gold content (2.6 wt.%) was determined by inductively coupled plasma atomic emission spectroscopy (ICP-AES) on a Varian Liberty 110 instrument. Solid samples pretreated at 350 °C in Ar flow for 30 min were first digested at room temperature in HF for 12 h and then in a mixture of HCl and HNO_3 for 30 min. The solution obtained was diluted with deionized water and analyzed.

The specific surface area was determined using the BET method by nitrogen thermal adsorption measurements in a Gemini 2600 Micromeritics device. Before analysis, the sample was heated in Ar flow at 300 °C for 1 h.

High-resolution transmission electron microscopy (HRTEM) was performed with a JEOL 2010 microscope. The sample was dispersed by ultrasonic in isopropanol and supported on a copper grid covered with carbon film. To determine the mean diameter of gold particles, more than 200 particles were chosen. The mean diameter (d_m) of particles was calculated using the following formula: $d_m = \frac{\sum_i (x_i d_i)}{\sum_i x_i}$, where x_i is the number of particles with diameter d_i.

In situ UV–Vis–Mass analysis of the transformation of gold species under temperature programmed reduction (TPR) was carried out in a lab-made set-up [39] with simultaneous analysis of gas phase components and recording of the UV–Vis spectra of the sample. UV–Vis spectra were collected using an AVANTES AvaSpec-2048 UV–Visible spectrometer equipped with an AvaLight-DHS light source and a high temperature optic fiber reflection probe located close to the external wall of the quartz reactor (i.d. 4 mm, o.d. 6 mm). UV–Vis spectra recorded each 15 s (time of spectrum recording was about 5 ms) were obtained by the subtraction of the initial spectrum recorded at room temperature from those recorded at elevated temperatures. The reactor packed with Al_2O_3 was used as the reference. The analysis of gas phase components was done in-line with an HPR20 mass spectrometer (Hiden). TPR was carried out under linear sample heating with a ramp rate of 20 °C min^{-1} up to 350 °C using a gas mixture consisting of H_2 (5 vol.%), Ar (5 vol.%), and He (balance). The relative content of the desorbed products was estimated considering all possible mass-fragments according to the Hiden mass-library, while hydrogen uptake was calculated using a reference gas mixture.

The extended X-ray absorption fine structure (EXAFS) and X-ray absorption near edge structure (XANES) spectra (transition and fluorescent modes) of the Au–L_3 edges for all the studied samples were obtained at the EXAFS Station of the Siberian Synchrotron Radiation Center in Novosibirsk (SSRC). The storage ring VEPP-3 with the electron beam energy of 2 GeV and the average stored current of 90 mA was used as the source of radiation. The X-ray energy was monitored with a channel cut Si(1 1 1) monochromator. The harmonic rejection was performed by using a SiO_2 mirror for all measurements. All EXAFS and XANES spectra were recorded with the steps of ca.1.5 eV and ca. 0.3 eV, respectively.

The EXAFS spectra were treated using the standard procedures [40,41]. The background was removed by extrapolating the pre-edge region onto the EXAFS region in the forms of polynomials. Three cubic splines were used to construct the smooth part of the absorption coefficient. The inflection point of the edge of the X-ray absorption spectrum was used as initial point ($k = 0$) of the EXAFS spectrum. The radial distribution of the atoms function (RDF) was calculated from the EXAFS spectra in $k^3\chi(k)$ by using Fourier transform in the wave number interval of 3.0–12.0 $Å^{-1}$. A curve fitting procedure with the EXCURV92 code [42] was employed to determine the distances and coordination numbers (CNs). It was realized for $k^3\chi(k)$ in similar wave number intervals after preliminary Fourier filtering using the known XRD literature data for the bulk compounds. The Debye–Waller factors were fixed: $2\sigma^2 = 0.009–0.013$ $Å^2$.

Photoelectron spectra were recorded using a SPECS spectrometer with a PHOIBOS-150 hemispherical energy analyzer and AlK_α irradiation ($h\nu = 1486.61$ eV, 200 W). A binding energy (BE) scale was preliminarily calibrated by the position of the peaks of Au $4f_{7/2}$ (84.0 eV) and Cu $2p_{3/2}$ (932.67 eV) core levels. The catalyst was mounted on a sample holder using a nickel grid to be able to heat a sample up to 500 °C. The BE of peaks was corrected to take into account a sample charging by referencing to the BE of the Mg 2s peak (88.9 eV) (internal standard). In addition to the survey, photoelectron spectra, more narrow spectral regions of Au 4f + Mg 2s, were recorded. For the survey spectra, the pass energy of the analyzer was 50 eV, while that for the narrow spectral regions was 20 eV.

2.3. Catalytic oxidation experiments

The reactions were carried out in a stainless steel reactor equipped with a magnetic stirrer. In a typical run, a mixture of the substrate (0.4–1.2 mmol), solvent (if any) (2 mL), and the catalyst (10–40 mg; ca. 0.6–2.4 wt.%; Au: 0.01–0.75 mol%) was transferred in the reactor. The reactor was pressurized with oxygen to the total pressure of 10 atm and placed in an oil bath; then, the solution was intensively stirred at 80–130 °C for the reported time. The reactions were followed by gas chromatography (GC) (Shimadzu 17 instrument, Carbowax 20 M capillary column). At appropriate time intervals, stirring was stopped and after catalyst settling aliquots were taken and analyzed by GC. To ensure correct GC results in solvent-free reactions and in those with high initial substrate concentrations, the aliquots were diluted with methanol before the analysis. The structures of the products were confirmed by GC/MS (Shimadzu QP2010-PLUS instrument, 70 eV).

3. Results and discussion

3.1. Activation and characterization of the catalyst

The UV–Vis spectrum of the freshly prepared Au/MgO catalyst is depicted in Fig. 1. The spectrum is characterized with the adsorption band at 350 nm (shown with arrow) which can be assigned to gold hydroxide species [43]. It is well established that the presence of metallic gold NPs could be easily detected with the band at ca. 520 nm, which is characteristic for the optical absorption of light excited oscillating conductivity electrons of metallic gold NPs: the so-called "plasmon resonance" [44]. The absence of this band in the spectrum shown in Fig. 1 provides a strong evidence for the absence of metal gold NPs in the freshly prepared Au/MgO sample.

However, metallic gold NPs of a hexagonal shape with a relatively small diameter (shown with white arrow in Fig. 2) were observed in TEM micrographs of the freshly prepared Au/MgO sample. These particles could be formed due to the decomposition of the gold precursor in a vacuum chamber of the electron microscope as it was observed in [13]. The size distribution of gold NPs in the freshly prepared Au/MgO sample is shown in Fig. 2. The estimated value of 2.3 nm seems to reflect the average size of the gold precursor agglomerates formed on the sample surface during the preparation procedures. No significant migration of the gold particles along the support surface is expected in the course of the reduction in the microscope due to relatively mild conditions. As

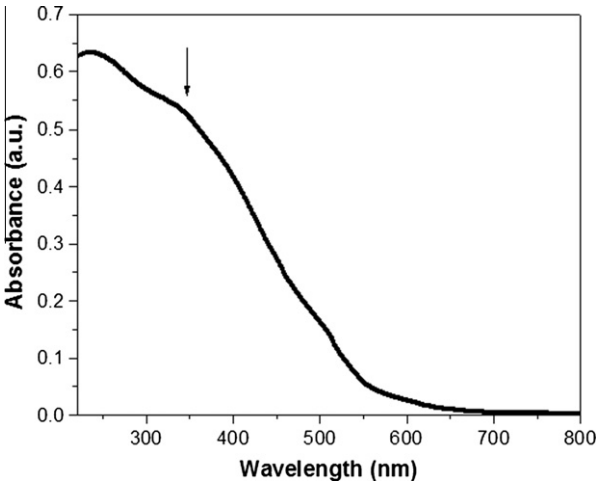

Fig. 1. UV–Visible spectrum of the freshly prepared Au/MgO sample.

the agglomerates of the precursor contain not only gold cations but also anionic species, they should be larger than the resulting particles of the metallic gold. Thus, we suggest that the size of the gold NPs formed on the surface of the freshly prepared Au/MgO catalysts during the TEM measurements is determined by the size of the precursor agglomerates.

TRP profiles and *in situ* UV–Vis–Mass spectra for the freshly prepared Au/MgO sample at TPR are presented in Fig. 3. Within the temperature range studied (up to 350 °C), a small hydrogen uptake as well as the desorption of H_2O, CO_2 and NH_3 was observed. In the UV–Vis spectra of the sample, the plasmon peak of metallic gold NPs centered in the range of 500–560 nm appeared under the TPR conditions, with the intensity and position of this peak being strongly depended on the temperature. The application of the *in situ* UV–Vis spectroscopy allowed monitoring the process of the formation of gold NPs in the course of TPR. The intensity of the plasmon peak increased significantly with the temperature rise indicating the increase in the amounts of gold NPs. The changes in the relative plasmon intensity, water desorption, and hydrogen uptake during the TPR are shown in Fig. 4. The profile of the plasmon intensity changes suggests that there are three distinguishable steps in the process of gold NPs formation: the first slow step at 50–180 °C, the second fast step at 180–225 °C, and the third slow step at 225–350 °C.

The first step proceeds with intense water evolving, albeit without any hydrogen consumption. Therefore, the formation of gold NPs at this step is determined by the thermal decomposition of the gold precursor ($Au(OH)_3 \rightarrow Au_2O_3 \rightarrow Au$) only. At this step, the formation of gold NPS is accompanied with a significant shift of the plasmon resonance (Fig. 4) which indicates the changes in the particle size. The peak position is shifted toward the red region of the spectrum which could be explained by the suggestion that growing gold NPs are coated with a layer of compounds characterized with a high value of dielectric function. Such an explanation is based on the theoretical estimations presented in [45]. Therefore, it can be suggested that gold NPs are formed in this temperature region mainly inside the primary particles of gold hydroxide, which have been supported on the MgO surface during the sample preparation.

The second step of the process, i.e., the fast formation of gold NPs within the narrow temperature interval of 180–225 °C, is accompanied by the hydrogen consumption (Fig. 4). However, the hydrogen uptake corresponds to only 0.05% of the value required for the complete reduction of the gold precursor. Therefore, the formation of gold NPs at this step mainly occurs also due to the thermal decomposition of the dehydrated gold deposit. Similarly to the previous step, significant changes in the plasmon position were observed suggesting that the formation of gold particles occurred with their agglomeration. The red shift of the plasmon position indicates that gold NPs formed at this step are still covered by a $Au(OH)_3$ layer.

In the course of the third step, the formation of gold NPs is being concluded. The low rate of this step is determined by the decomposition of the residual part of the gold precursor. The reduction with hydrogen of the external surface of the gold deposit particles at 225 °C provokes the desorption of ammonia. The latter indicates that at this point, the $Au(OH)_3$ film, which covers the gold nanoparticles, is completely reduced to Au^0 causing the desorption of ammonia because of its lower affinity toward the metallic gold compared to gold hydroxide. A further temperature increase up to 350 °C does not affect the position of plasmon indicating stability of the gold NPs toward sintering under these conditions.

TEM images of the reduced Au/MgO sample are presented in Fig. 5. The gold NPs formed under the sample reduction described above are characterized with a quasi spherical shape. The comparison of the TEM images for the freshly prepared and reduced Au/

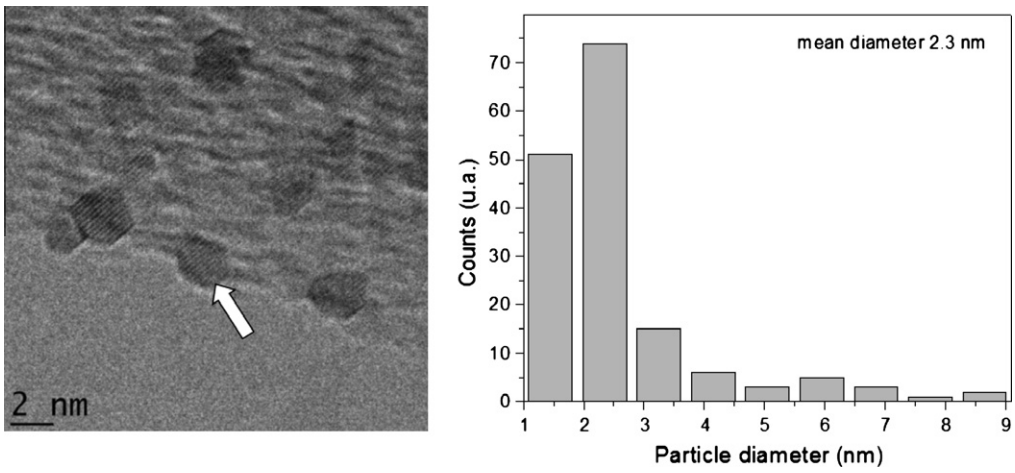

Fig. 2. TEM data for the freshly prepared Au/MgO sample: the TEM micrograph (on the left), the histogram of the gold NPs distribution in size (on the right).

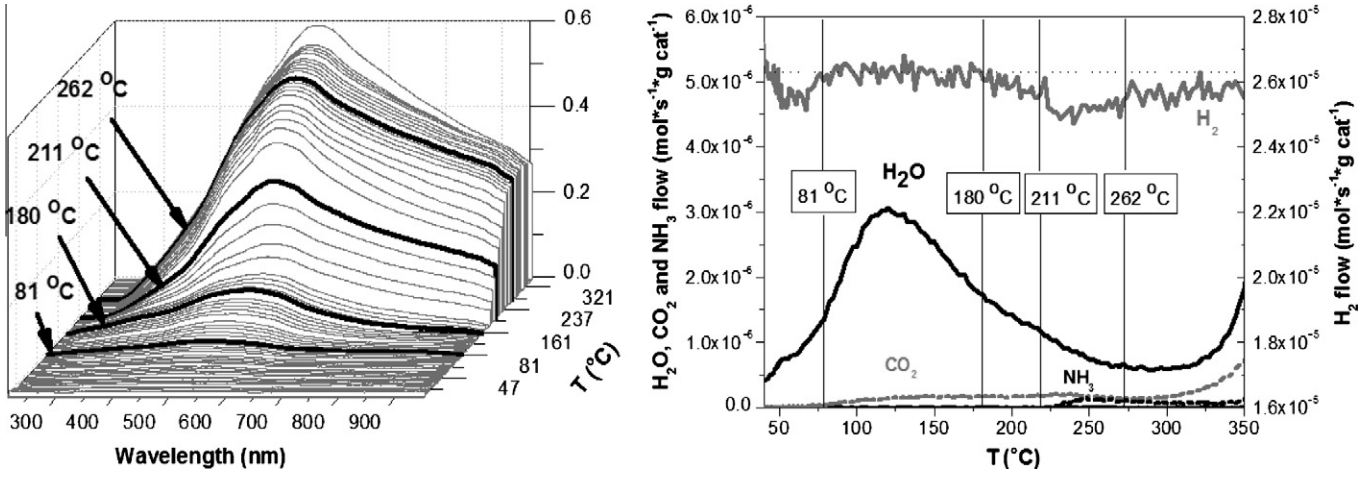

Fig. 3. In situ-UV–Vis–Mass analysis of the freshly prepared Au/MgO sample at TPR (on the left: UV–Vis spectra; on the right: TPR profiles).

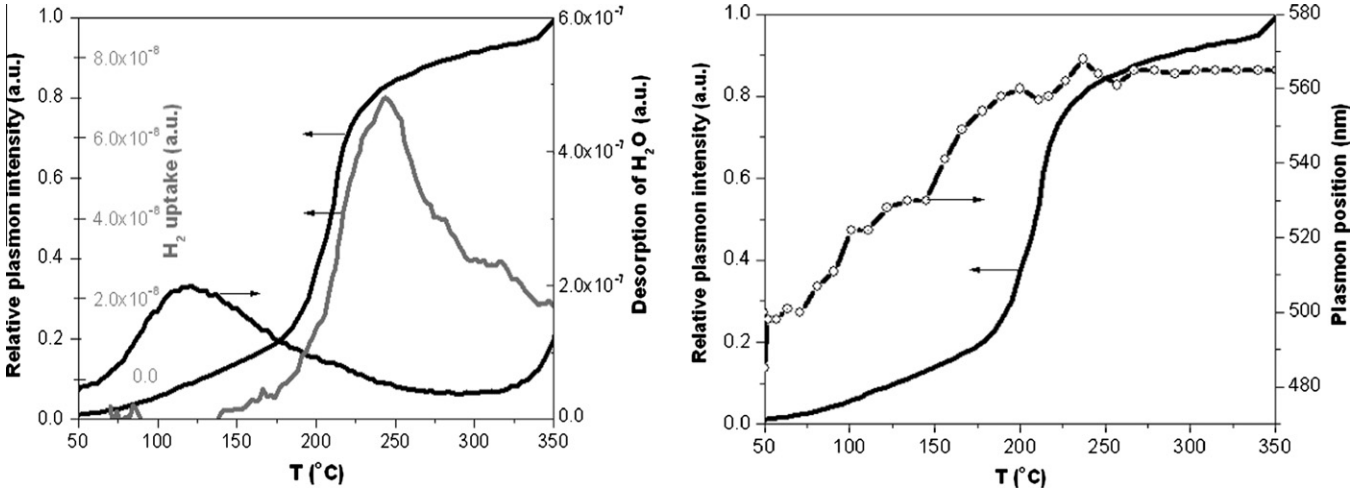

Fig. 4. TPR analysis of the freshly prepared Au/MgO. Hydrogen uptake, water desorption, and relative plasmon intensity vs. temperature (on the left). Relative plasmon intensity and plasmon position vs. temperature (on the right).

MgO samples showed that the sample treatment at high temperature (up to 350 °C) resulted in the agglomeration of the particles. Their average diameter was found to be equal to 3.4 nm (Fig. 5).

The surface analysis of the reduced Au/MgO sample by X-ray photoelectron spectroscopy (XPS) was used to clarify the chemical state of the gold species formed on the catalyst surface. The XP

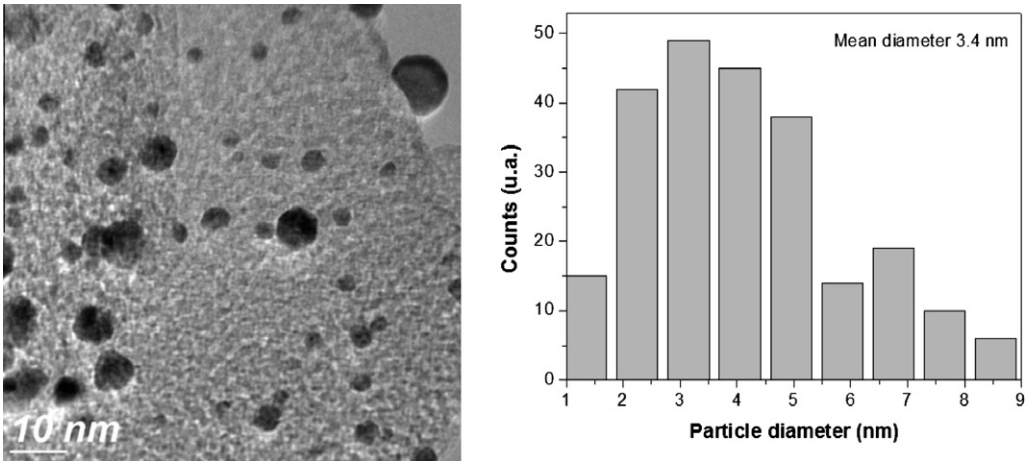

Fig. 5. TEM data for the reduced Au/MgO sample: the TEM micrograph (on the left), the histogram of the gold NPs distribution in size (on the right).

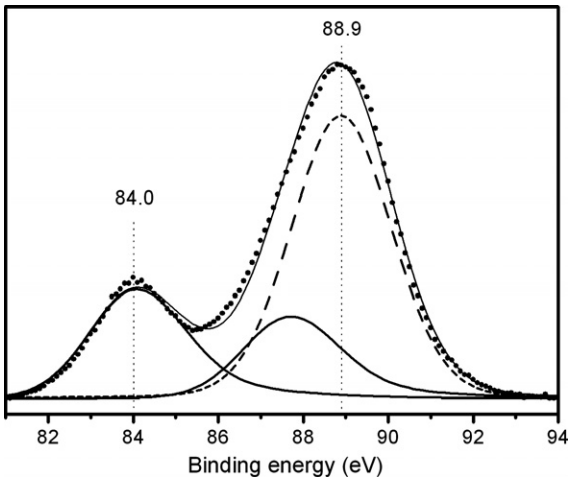

Fig. 6. The experimental XP spectrum (dots) and the results of fitting of the Mg 2s (dashed line) and Au 4f region (solid lines) for the reduced Au/MgO catalyst.

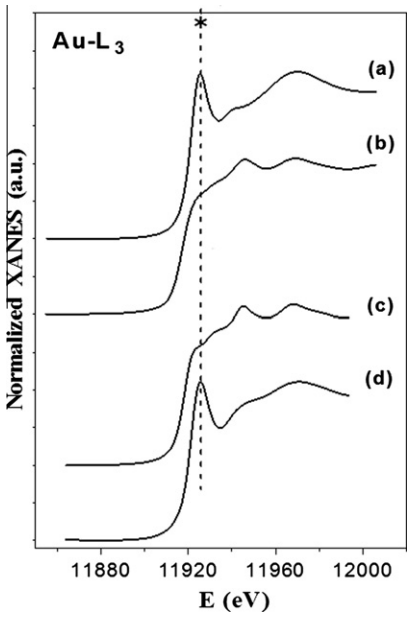

Fig. 7. The XANES spectra (Au–L_3) of the samples studied: (a) the freshly prepared Au/MgO; (b) the reduced Au/MgO; (c) the reference Au foil; (d) the reference oxide, Au_2O_3 [34]. Au–L_3 edge,* – white line.

spectrum for Mg 2s and Au 4f regions is presented in Fig. 6. The spectrum for Au 4f is characterized only by one doublet of two spin–orbit components separated by 3.67 eV, i.e., Au $4f_{7/2}$ and Au $4f_{5/2}$, which can be attributed to metallic gold species according to [46].

The evolution of the chemical and coordination state of the gold species at the catalyst preparation was verified by X-ray absorption spectroscopy (XAS). The normalized XANES spectra for the freshly prepared and reduced Au/MgO samples, the reference Au-foil and Au_2O_3 from [47], are shown in Fig. 7. The XANES spectrum of the freshly prepared Au/MgO sample (Fig. 7a) is similar to that of Au_2O_3 (Fig. 7d), with only minor differences being observed. The high amplitude of the white line clearly indicates the presence of the oxidized phase [48]; thus, the main part of the gold species in both freshly prepared Au/MgO and Au_2O_3 samples presents as Au^{3+} cations in oxygen surrounding. The XANES spectrum of the reduced Au/MgO sample (Fig. 7b) is similar to that of the reference Au-foil (Fig. 7c). The amplitude of the white line is quite low in both materials. Thus, gold mainly presents in the reduced Au/MgO sample as the Au^0 metallic phase.

The RDFs describing the Au local arrangements for the samples are shown in Fig. 8. The RDF for the reference Au-foil (Fig. 8c) is typical for the face-centered cubic (fcc) structure, with the main peak corresponding to the shortest Au–Au distance (R_{Au-Au} = 2.87 Å, CN = 12) [49]. Fitting performed as described in Experimental gives very close values for R_{Au-Au} (ca. 2.86 Å) and CN (ca. 12.0).

The main peak in the RDF for the freshly prepared Au/MgO sample, which is located at ca. 1.2–2.2 Å, can be attributed to the Au–O distance of ca. 2.0 Å (Fig. 8a) [50,51]. Fitting gives the following set of values: $R_{Au-O} \approx 1.99$ Å and CN ≈ 5.9–6.0. Thus, only Au^{3+}cations present in this sample in nearly octahedral oxygen surrounding. This Au hydroxide–oxide structure is different from the bulk Au_2O_3 oxide where Au^{3+}cations are in four-coordinated positions [50]. No metallic gold species were detected in the freshly prepared Au/MgO sample within the method limit. The results obtained are in a good agreement with the UV–Vis data for this sample.

The shape of the RDF for the reduced Au/MgO sample (Fig. 8d) is in general similar to that for the Au-foil with the fcc structure; however, the amplitude of the first Au–Au peak located at ca. 1.7–3.5 Å is slightly lower. Fitting gives the values of ca. 2.84 Å for R_{Au-Au} and 8.2–8.5 for CN, which are fully consistent with the correlation between the Au–Au coordination number and the

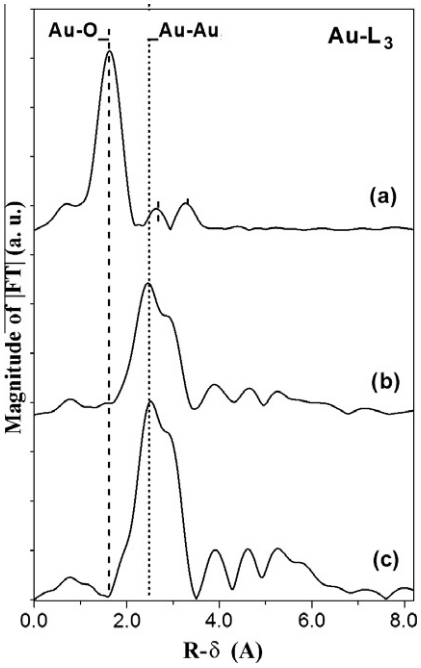

Fig. 8. The curves of the radial distribution function of atoms (RDF) describing the gold local arrangement for the samples studied: (a) the freshly prepared Au/MgO; (b) the reduced Au/MgO; (c) the reference Au foil.

interatomic Au–Au bond length determined by van Bokhoven et al. [52]. The decrease in the coordination number compared to Au foil may be explained by the distortions of the metal fcc structure and nano-size effects [53]. No Au^{3+} species were detected in the reduced Au/MgO sample within the method limit.

The XAS (XANES/EXAFS) results obtained for the reduced Au/MgO sample are in a good agreement with the XPS and TEM data. The size of the Au particle may be estimated from the previously reported correlation between the coordination number and the particle size [54]. The obtained value correlates well with the TEM data (Fig. 5) implying that the reduced Au/MgO sample contains no significant amount of small gold particles (less than 1 nm) which cannot be observed by the TEM techniques. In other words, the histogram presented in Fig. 5 represents well the size distribution of most of the gold particles present on the surface of the reduced Au/MgO sample.

3.2. Catalytic studies

The catalytic activity of the reduced Au/MgO sample in the oxidation of benzyl alcohol (**1a**) was tested in methanol solutions under the atmosphere of molecular oxygen. In all experiments, this material was applied as a sole catalyst in the absence of any co-catalysts or additives. The results are presented in Table 1.

It was found that Au/MgO effectively catalyzed the oxidative esterification of benzyl alcohol showing high activity, whereas in the presence of pure support or without any catalyst added, the conversion of the substrate was negligible. The reaction resulted in two major products: benzaldehyde **1b** and methyl benzoate **1c** (Scheme 1). A combined selectivity for these two products was 90–100% in all the runs, with only small amounts of benzoic acid and benzyl benzoate being detected in reaction solutions. Methyl benzoate and benzyl benzoate are formally the products of the esterification of benzoic acid with methanol and benzyl alcohol, respectively. The relative amounts of the products **1b** and **1c** depended on the reaction time, with the ester **1c** being a predominant product at the end of the reaction.

The reactions occurred with very low catalyst loadings (0.6 wt.%) so that turnover numbers (TONs) reached high values (up to ca. 30.000) reflecting high stability of the catalyst. The catalyst is a solid material that is insoluble in the reaction mixture; it can be separated from the products by simple centrifugation or filtration. These features represent the important technological advantages of the process.

The oxidation of benzyl alcohol in the presence of Au/MgO readily occurred at 100 °C resulting in a complete conversion in 3 h to give almost exclusively methyl ester **1c** (92%) along with aldehyde **1b** (8%, Table 1, run 1). Keeping the mixture under stirring up to 6 h resulted in the almost complete conversion of aldehyde **1b** to give ester **1c**, which was obtained at the end of the reaction in a virtually quantitative yield.

To increase the catalyst efficiency in terms of turnover numbers (TONs), the amount of the substrate was doubled (Table 1, runs 2 and 3). In these runs, it can be clearly seen the increase in ester selectivity with the reaction time. In run 2, a virtually complete conversion of the substrate was observed for 6 h; however, benzaldehyde **1b** accounted for ca. 30% of the products. At longer reaction time, most of the aldehyde was converted in the methyl ester, which is consistent with a two-step mechanism involving the oxidation of alcohol to aldehyde and further oxidation of aldehyde to ester (see below). In run 3, ester **1c** was obtained in a virtually quantitative yield.

The results of runs 2 and 3 (Table 1) correspond to the TON of nearly 20.000 with respect to the surface amounts of gold; i.e., the fraction of the gold atoms that are located on the surface of the gold particles and are, therefore, accessible for the substrate. The surface amounts of Au (8.47% of the total amounts) can be calculated based on the average particle diameter (3.4 nm) determined by TEM as the XAS study has confirmed that the reduced Au/MgO material contains no appreciable amounts of the Au particles smaller than 1 nm.

The performance of the Au/MgO catalyst in the oxidative esterification of benzyl alcohol is comparable with that of the Au/HMS catalysts reported in our previous work [30]. However, the Au/HMS systems required a base co-catalyst (potassium carbonate): in the absence of base, no conversion of the alcohol was observed. The important advantage of the Au/MgO catalyst is no need in base, the catalyst is active in the absence of any base co-catalyst added. In run 4, which was performed under the same conditions used in [30], however, without the base, the reaction showed the initial turnover frequency (TOF) of 155 min^{-1} and TON of nearly 32.000. These results compare well with most of the reported catalysts and put the prepared material among the best gold catalysts developed for the oxidative methoxylation of benzyl alcohol [25,27–29]. The catalyst after run 3 in Table 1 was reused converting another portion of the substrate without a significant loss of activity and selectivity.

Although the reaction occurs smoothly with Au/MgO as the sole catalyst, the addition of potassium carbonate (0.16 equiv.) increases the rate of both reaction steps: the oxidation of benzyl alcohol to benzaldehyde and further oxidation of the latter into the ester (cf. run 6 and 5 in Table 1).

It should be emphasized that in the presence of Au/MgO, benzyl alcohol can be oxidized by molecular oxygen without any solvent, i.e., in a solvent-free system (Table 2, runs 1 and 2). However, high selectivity for benzaldehyde has been obtained only at low substrate conversions. Then, a significant difference in a mass balance was observed due to the formation of oligomers, which were not CG determinable.

The mechanism proposed for the oxidative esterification of primary alcohols involves as the first step the oxidation of the alcohol into the aldehyde followed by the condensation reaction between the aldehyde and alcohol resulting in hemiacetal [26,28]. The lat-

Table 1
Oxidation of benzyl alcohol (**1a**) catalyzed by Au/MgO in methanol solutions.[a]

Run	Substrate (mmol)	Temperature (°C)	Time (h)	Conversion (%)	Product selectivity (%)		TON[b]	TOF[c] (min^{-1})
					Aldehyde **1b**	Ester **1c**		
1	0.4	100	3	100	8	92		
			6	100	2	98	7.084	n.d.
2	1.2	110	6	98	31	64		
			10	100	12	83	19.415	n.d.
3[d]	1.2	120	1	64	57	42		
			8	100	2	98	21.595	n.d.
4	2.5	110	1	38	67	27		
			10	96	33	58	32.494	155
5	2.5	100	1	16	58	28		
			9	75	44	48	23.843	68
6[e]	2.5	100	1	40	45	46		
			6	95	3	87	38.751	148

[a] Conditions: catalyst 2.6 wt.% Au/MgO (10 mg, ca. 0.6 wt.%); methanol (2 mL); 10 atm (O_2). Conversion and selectivity were determined by GC; n.d. – not determined.
[b] Turnover number (TON) is calculated as a ratio between the amounts of **1b** and **1c** formed and the surface amounts of Au, considering that **1c** is formed from **1a** via **1b** and both steps are catalyzed by Au: TON = [n(**1b**)+2n(**1c**)]/n (Au), where n represents the amount of the indicated compound or Au in moles. The surface amounts of Au correspond to 8.47% of the total amounts (calculated based on the average particle diameter of 3.4 nm).
[c] Initial rate of the substrate conversion per mol of Au (initial turnover frequency).
[d] The catalyst was reused after this run without a significant loss of activity and selectivity.
[e] K_2CO_3 – 0.4 mmol.

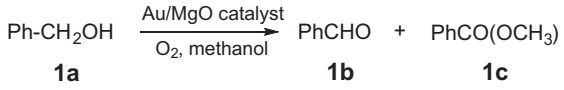

Scheme 1. Oxidation of benzyl alcohol **1a** into benzaldehyde **1b** and methyl benzoate **1c**.

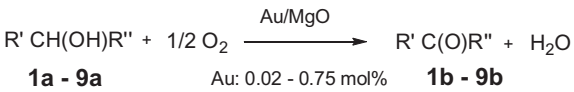

Scheme 2. Oxidation of natural alcohols into corresponding aldehydes or ketones.

ter, which is considered as a key intermediate of the process, undergoes then dehydrogenation to give the ester. Small amounts of benzoic acid detected in the reaction solutions could be the result of the dehydrogenation of a hydrate formed by the interaction of the aldehyde with trace water instead of methanol. The formation of the hemiacetal as a reaction intermediate has been also suggested to explain the formation of benzyl benzoate at the solvent-free oxidation of benzyl alcohol over gold catalysts [17].

The activity of the Au/MgO material was also examined in the aerobic oxidation of a wide variety of primary and secondary alcohols, including sterically hindered cyclic alcohols. In all experiments, this material was also applied as a sole catalyst in the absence of base co-catalysts. Corresponding aldehyde and ketones were detected as major, often exclusive, products of these reactions (Scheme 2). Representative results are collected in Table 2.

A secondary benzylic alcohol, 1-phenylpropanol (**2a**), can be oxidized over Au/MgO to give corresponding ketone **2b** (Scheme 3) in a solvent-free system (Table 2, run 3) as well as in methanol or toluene solutions (Table 2, runs 4–6). It should be mentioned that the reaction occurs much faster in methanol than in toluene

Table 2
Oxidation of alcohols catalyzed by Au/MgO.[a]

Run	Substrate (mmol)	Solvent	Catalyst (mg)	Temperature (°C)	Time (h)	Conversion (%)	Product	Selectivity (%)	TON[b]
1[c]	Benzyl alcohol (**1a**)	None	20	100	4	15	**1b**	100	12.262
2[c]	Benzyl alcohol (**1a**)	None	20	120	4	44	**1b**	65	35.970
3[c]	1-Phenylpropanol (**2a**)	None	10	120	8	30	**2b**	95	20.436
4	1-Phenylpropanol (**2a**)	Methanol	10	130	2	97	**2b**	100	3.543
5[d]	1-Phenylpropanol (**2a**)	Methanol	10	110	2	73	**2b**	100	
					8	90	**2b**	100	9.809
6[d]	1-Phenylpropanol (**2a**)	Toluene	10	110	2	40	**2b**	100	3.778
7	Nerol (**3a**)	Methanol	10	80	8	50	**3b**	90	1.812
8	Nerol (**3a**)	Toluene	10	80	8	25	**3b**	85	900
9[d]	Perillyl alcohol (**4a**)	Methanol	20	110	7	90	**4b**	97	4.905
10[d]	Isoborneol (**5a**)	Methanol	40	110	10	98	**5b**	100	2.725
11	Carveol (**6a**)	Methanol	20	120	8	86	**6b**	100	1.567
12	Carveol (**6a**)	Toluene	20	120	8	76	**6b**	100	1.362
13	Menthol (**7a**)	Methanol	10	130	8	12	**7b**	100	408
14	Isopulegol (**8a**)	Methanol	20	120	8	34	**8b**	80	613
15	Citronellol (**9a**)	Methanol	20	120	8	20	**9b**	46	340

[a] Conditions: substrate (0.4 mmol), solvent (2 mL), 10 atm (O_2), catalyst contains 2.6 wt.% of Au. Conversion and selectivity were determined by GC.
[b] TON – moles of the substrate converted/moles of Au. TON was calculated with respect to the surface amounts of gold (8.47% of the total amounts as calculated from the average particle diameter of 3.4 nm).
[c] Substrate – 2 mL (18 mmol of **1a** or 15 mmol of **2a**).
[d] Substrate – 1.2 mmol.

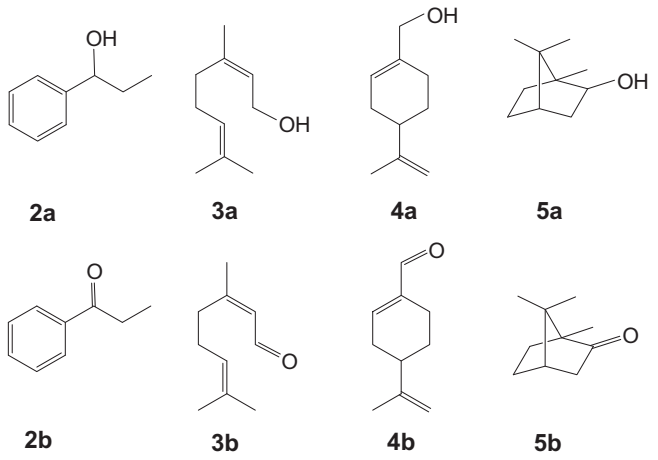

Scheme 3. Structures of alcoholic substrates **2a**–**5a** and corresponding products **2b**–**5b**.

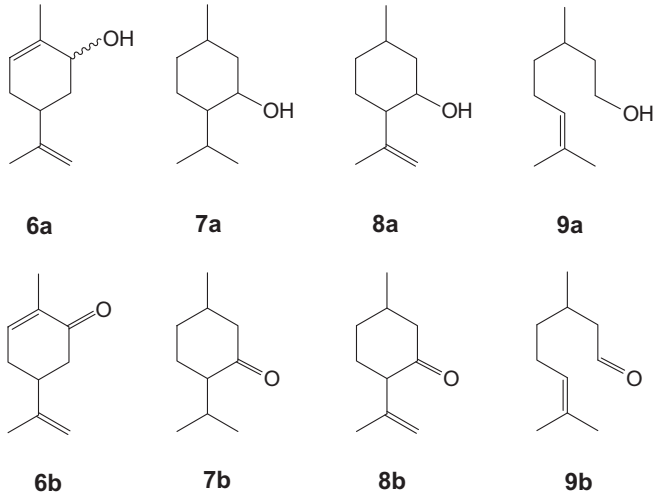

Scheme 4. Structures of alcoholic substrates **6a**–**9a** and corresponding products **6b**–**9b**.

(Table 2, cf. runs 5 and 6), a tendency that has been later confirmed by the study with other alcohols.

In a further work, the Au/MgO catalyst was tested for the aerobic oxidation of various natural monoterpenic alcohols in order to clarify the substrate scope and to synthesize carbonylic terpenoids important for fragrance and pharmaceutical industries. With most of the alcohols, the reaction conditions were varied to achieve better yields for corresponding aldehydes or ketones. The results of the runs with the best yields are presented in Table 2.

Nerol (**3a**), a monoterpenic primary allylic alcohol available from many essential oils, was oxidized over the Au/MgO catalyst giving as a major product (*Z*)-citral (**3b**), an important aroma compound with a strong lemon odor (Table 2, runs 7 and 8; Scheme 3). Citral was obtained with 90% selectivity at 50% conversion of nerol. The reaction was much slower in toluene solutions, like it was observed with 1-phenylpropanol (Table 2, cf. runs 7 and 8).

The oxidation of another monoterpenic primary allylic alcohol, perillyl alcohol (**4a**), occurred with an excellent selectivity to give perillyl aldehyde (**4b**) in nearly quantitative yield (Scheme 2; Table 2, run 9). Perillyl aldehyde, which is much more expensive than original alcohol **4a**, is used as food additive for flavoring and in perfumery to add spiciness.

The oxidation of sterically hindered isoborneol (**5a**) over Au/MgO material gives almost quantitatively camphor (**5b**) (Scheme 3), a compound with a strong, aromatic odor used as a local analgesic, respiratory stimulant, plasticizer and an antimicrobial agent (Table 2, run 10).

The Au/MgO catalyst is also very effective for the oxidation of the commercial (Sigma–Aldrich) mixture of *trans* and *cis* isomers of carveol (**6a**) resulting in carvone (**6b**) with ca. 100% selectivity (Scheme 4, Table 2, runs 11 and 12). Similarly to what has been observed with other substrates, the reaction is faster in methanol solutions than in toluene (Table 2, cf. runs 11 and 12). Thus, we can conclude that methanol is a better solvent than toluene to perform the oxidation of alcohols over the Au/MgO catalyst. Carveol **6a** and perillyl alcohol **4a** are both allylic alcohols with a *para*-menthenic skeleton; however, carveol is a secondary alcohol. A similar reaction rate was attained for carveol at higher temperature and higher catalyst loading as compared to perillyl alcohol, probably, due to the steric hindrance of the hydroxyl group (Table 2, cf. runs 9 and 11). The results obtained for substrates **3a**, **4a** and **6a** suggest that the Au/MgO catalyst promotes selective transformations of α,β-unsaturated alcohols into corresponding α,β-unsaturated aldehydes or ketones without intramolecular hydrogen transfer and isomerization.

Non-activated monoterpenic alcohols, menthol (**7a**), isopulegol (**8a**), and citronellol (**9a**) (Scheme 4) were much less reactive toward oxidation under similar conditions than their activated counterparts, carveol, and nerol. Although the reactions with **7a** and **8a** were selective to corresponding ketones (menthone **7b** and isopulegone **8b**), low conversions were attained under relatively drastic conditions (120–130 °C, 8 h, Table 2, runs 13–15). It should be mentioned that no formation of the corresponding methyl esters has been observed at the oxidation of primary alcohols **3a**, **4a,** and **9a**, whereas the oxidation of benzyl alcohol under similar conditions gives mainly methyl benzoate. The reasons for such a different behavior of these substrates are not clear yet and need further investigation.

4. Conclusions

Monitoring the formation of gold nanoparticles on the surface of magnesium oxide has revealed, for the first time as far as we know, that the process occurs through three distinguishable steps of the thermal decomposition of gold hydroxide, which are accompanied by negligible hydrogen consumption. Stabilization of gold hydroxide particles with ammonia hydroxide at the Au/MgO preparation resulted in the formation of truly uniform gold nanoparticles. The material is an effective heterogeneous catalyst for the liquid-phase oxidation of a wide range of alcohols with environmentally benign molecular oxygen, in the absence of any co-catalyst or additive. In addition, the Au/MgO catalyst performs the one-pot base-free aerobic oxidative esterification of benzyl alcohol exhibiting high activity, selectivity to methyl benzoate and stability. The oxidation of various biomass-based monoterpenic alcohols over the Au/MgO catalyst resulted in carbonylic terpenoids, useful for fragrance and pharmaceutical industries, in good to excellent yields.

Acknowledgments

The authors thank E. Flores, A. Diaz, P. Casillas, V. Garcia, M. Sainz, F. Ruiz, G. Vilchis, E. Aparicio, J. Peralta, J. Palomares, and M. Vega for technical support. This research project was partly supported by DGAPA-PAPIIT (UNAM, México) through Grant IN 224510 and by CNPq, CAPES, FAPEMIG and INCT-Catálise (Brazil).

References

[1] R.A. Sheldon, I.W.C.E. Arends, A. Dijksman, Catal. Today 57 (2000) 157.
[2] J. Muzart, Tetrahedron 59 (2003) 5789.
[3] M.J. Schultz, M.S. Sigman, Tetrahedron 62 (2006) 8227.
[4] K. Mori, T. Hara, T. Mizugaki, K. Ebitani, K. Kaneda, J. Am. Chem. Soc. 126 (2004) 10657.
[5] T. Mallat, A. Baiker, Chem. Rev. 104 (2004) 3037.
[6] T. Nishimura, N. Kakiuchi, M. Inoue, S. Uemura, Chem. Commun. (2000) 1245.
[7] K. Yamaguchi, N. Mizuno, Angew. Chem., Int. Ed. 41 (2002) 4538.
[8] T. Matsushita, K. Ebitani, K. Kaneda, Chem. Commun. (1999) 265.
[9] V.V. Costa, M.J. Jacinto, L.M. Rossi, R. Landers, E.V. Gusevskaya, J. Catal. 282 (2011) 209.
[10] L. Prati, M. Rossi, J. Catal. 176 (1998) 552.
[11] C. Della Pina, E. Falletta, L. Prati, M. Rossi, Chem. Soc. Rev. 37 (2008) 2077.
[12] G.J. Hutchings, Chem. Commun. (2008) 1148.
[13] A. Corma, H. Garcia, Chem. Soc. Rev. 37 (2008) 2096.
[14] V.R. Choudhary, D.K. Dumbre, Catal. Commun. 13 (2011) 82.
[15] S. Meenakshisundaram, E. Nowicka, P.J. Miedziak, G.L. Brett, R.L. Jenkins, N. Dimitratos, S.H. Taylor, D.W. Knight, D. Bethell, G.J. Hutchings, Faraday Discuss. 145 (2010) 341.
[16] D.I. Enache, J.K. Edwards, P. Landon, B. Solsona-Espriu, A.F. Carley, A.A. Herzing, M. Watanabe, C.J. Kiely, D.W. Knight, G.J. Hutchings, Science 311 (2006) 362.
[17] V.R. Choudhary, D.K. Dumbre, Top. Catal. 52 (2009) 1677.
[18] M. Sankar, E. Nowicka, R. Tiruvalam, Q. He, S.H. Taylor, C.J. Kiely, D. Bethell, D.W. Knight, G.J. Hutchings, Chem. Eur. J. 17 (2011) 6524.
[19] M. Boronat, A. Corma, F. Illas, J. Radilla, T. Ródenas, M.J. Sabater, J. Catal. 278 (2011) 50.
[20] P. Haider, J.-D. Grunwaldt, A. Baiker, Catal. Today 141 (2009) 349.
[21] G.L. Brett, Q. He, C. Hammond, P.J. Miedziak, N. Dimitratos, M. Sankar, A.A. Herzing, M. Conte, J.A. Lopez-Sanchez, C.J. Kiely, D.W. Knight, S.H. Taylor, G.J. Hutchings, Angew. Chem. Int. Ed. 50 (2011) 10136.
[22] A. Villa, G.M. Veith, L. Prati, Angew. Chem. Int. Ed. 49 (2010) 4499.
[23] M. Alhumaimess, Z. Lin, W. Weng, N. Dimitratos, N.F. Dummer, S.H. Taylor, J.K. Bartley, C.J. Kiely, G.J. Hutchings, ChemSusChem 5 (2012) 125.
[24] S.K. Klitgaard, A.T. DeLa Riva, S. Helveg, R.M. Werchmeister, C.H. Christensen, Catal. Lett. 126 (2008) 213.
[25] T. Hayashi, T. Inagaki, N. Itayama, H. Baba, Catal. Today 117 (2006) 210.
[26] I.S. Nielsen, E. Taarning, K. Egeblad, R. Madsen, C.H. Christensen, Catal. Lett. 116 (2007) 35.
[27] E. Taarning, A.T. Madsen, J.M. Marchetti, K. Egeblad, C.H. Christensen, Green Chem. 10 (2008) 408.
[28] F.-Z. Su, J. Ni, H. Sun, Y. Cao, H.-Y. He, K.-N. Fan, Chem. Eur. J. 14 (2008) 7131.
[29] H. Miyamura, T. Yasukawa, S. Kobayashi, Green Chem. 12 (2010) 776.
[30] L.A. Parreira, N. Bogdanchikova, A. Pestryakov, T.A. Zepeda, I. Tuzovskaya, M.H. Farías, E.V. Gusevskaya, Appl. Catal. A 397 (2011) 145.
[31] L. Menini, M.C. Pereira, L.A. Parreira, J.D. Fabris, E.V. Gusevskaya, J. Catal. 254 (2008) 355.
[32] P.A. Robles-Dutenhefner, K.A. da Silva Rocha, E.M.B. Sousa, E.V. Gusevskaya, J. Catal. 265 (2009) 72.
[33] M.G. Speziali, P.A. Robles-Dutenhefner, E.V. Gusevskaya, Organometallics 26 (2007) 4003.
[34] M.G. Speziali, V.V. Costa, P.A. Robles-Dutenhefner, E.V. Gusevskaya, Organometallics 28 (2009) 3186.
[35] L.A. Parreira, L. Menini, J.C. da Cruz Santos, E.V. Gusevskaya, Adv. Synth. Catal. 352 (2010) 1533.
[36] P.A. Robles-Dutenhefner, B.N.S. Brandao, L.F. de Sousa Liniker, E.V. Gusevskaya, Appl. Catal. A 399 (2011) 172.
[37] R. Zanella, S. Giorgio, C.R. Henry, C. Louis, J. Phys. Chem. 106 (2002) 7634.
[38] S.I. Ivanova, C. Petit, V. Pitchon, Catal. Today 113 (2006) 182.
[39] Yu.S. Solkina, S.I. Reshetnikov, M. Estrada, A. Simakov, D.Yu. Murzin, I.L. Simakova, Chem. Eng. J. 176–177 (2011) 42.
[40] D.I. Kochubey, EXAFS Spectroscopy of Catalysts, Nauka, Novosibirsk, 1992.
[41] K.V. Klementiev, code VIPER for Windows, freeware. <www.desy.de/~klmn/viper.html>.
[42] N. Binsted, J.V. Campbell, S.J. Gurman, P.C. Stephenson, EXCURV92 Program Code, SERC Daresbury Laboratory, UK, 1991.
[43] E. Smolentseva, A. Simakov, S. Beloshapkin, M. Estrada, E. Vargas, V. Sobolev, R. Kenzhin, S. Fuentes, Appl. Catal. B 115–116 (2012) 117.
[44] D.L. Feldheim, C.A. Foss, Metal Nanoparticles: Synthesis, Characterization and Applications, Basel Marsel Dekker Inc., New York, 2002.
[45] I. Tuzovskaya, N. Bogdanchikova, A. Simakov, V. Gurin, A. Pestryakov, M. Avalos, M. Farias, Chem. Phys. 338 (2007) 23.
[46] J.F. Moulder, W.F. Stickle, P.E. Sobol, K.D. Bomben, Handbook of X-ray Photoelectron Spectroscopy, Perkin-Elmer Corporation, Physical Electronics Division, Eden Prairie, 1992. p. 179.
[47] N. Weiher, E. Bus, L. Delannoy, C. Louis, D.E. Ramaker, J.T. Miller, J.A. van Bokhoven, J. Catal. 240 (2006) 100.
[48] H. Yoshida, S. Nonoyama, Y. Yazawa, T. Hattori, Phys. Scr. T115 (2005) 813.
[49] ICSD Database Code 64701-Au0.
[50] ICSD Database Code 8014-Au2O3.
[51] ICSD Database Code 64701-AuAlO2.
[52] J.T. Miller, A.J. Kropf, Y. Zha, J.R. Regalbuto, L. Delannoy, C. Louis, E. Bus, J.A. van Bokhoven, J. Catal. 240 (2006) 222.
[53] R.E. Benfield, J. Chem. Soc. Faraday Trans. 88 (1992) 1107.
[54] A.I. Frenkel, C.W. Hills, R.G. Nuzzo, J. Phys. Chem. 105 (2001) 12689.